REGULAR ARTICLE

blood advances

The endothelial glycocalyx anchors von Willebrand factor fibers to the vascular endothelium

Thejaswi Kalagara,[1,2,*] Tracy Moutsis,[1,*] Yi Yang,[1,3] Karin I. Pappelbaum,[1] Anne Farken,[1] Lucia Cladder-Micus,[2] Sabine Vidal-y-Sy,[4] Axel John,[5] Alexander T. Bauer,[4] Bruno M. Moerschbacher,[2] Stefan W. Schneider,[4] and Christian Gorzelanny[1,4]

[1]Department of Dermatology, Medical Faculty Mannheim, Heidelberg University, Mannheim, Germany; [2]Institute for Biology and Biotechnology of Plants, University of Münster, Münster, Germany; [3]Department of Orthopedics, Tongji Hospital, Tongji University School of Medicine, Shanghai, China; [4]Department of Dermatology and Venereology, University Hospital Hamburg-Eppendorf, Hamburg, Germany; and [5]Department of Urology, University of Ulm, Ulm, Germany

Key Points

- The endothelial glycocalyx controls platelet recruitment through the tethering of VWF.
- Glycocalyx shedding attenuates VWF fiber formation in melanoma.

The dynamic change from a globular conformation to an elongated fiber determines the ability of von Willebrand factor (VWF) to trap platelets. Fiber formation is favored by the anchorage of VWF to the endothelial cell surface, and VWF-platelet aggregates on the endothelium contribute to inflammation, infection, and tumor progression. Although P-selectin and αvβ3-integrins may bind VWF, their precise role is unclear, and additional binding partners have been proposed. In the present study, we evaluated whether the endothelial glycocalyx anchors VWF fibers to the endothelium. Using microfluidic experiments, we showed that stabilization of the endothelial glycocalyx by chitosan oligosaccharides or overexpression of syndecan-1 (SDC-1) significantly supports the binding of VWF fibers to endothelial cells. Heparinase-mediated degradation or impaired synthesis of heparan sulfate (HS), a major component of the endothelial glycocalyx, reduces VWF fiber–dependent platelet recruitment. Molecular interaction studies using flow cytometry and live-cell fluorescence microscopy provided further evidence that VWF binds to HS linked to SDC-1. In a murine melanoma model, we found that protection of the endothelial glycocalyx through the silencing of heparanase increases the number of VWF fibers attached to the wall of tumor blood vessels. In conclusion, we identified HS chains as a relevant binding factor for VWF fibers at the endothelial cell surface in vitro and in vivo.

Introduction

von Willebrand factor (VWF) is produced and stored in endothelial cells as a large multimeric protein with a molecular weight of up to several gigadaltons.[1] Various compounds, such as histamine and thrombin, induce the instantaneous secretion of VWF from the endothelium into the blood flow, which exposes the protein to shear stress. This leads to the elongation of VWF and thus to the formation of adhesive fiber networks. These fibers can tether circulating platelets to the endothelium as part of the processes of coagulation, inflammation, and tumor progression.[2-5]

The binding of circulating platelets is mediated by the A1 domain of VWF. This domain is hidden in nonstretched VWF but becomes accessible after VWF elongation. The critical shear force that is required to induce the conformational change of VWF is largely dependent on the localization of the VWF molecule. Free-floating, plasmatic VWF is stretched at a shear rate of ~2000 s^{-1}.[6] Elongation of VWF attached to the vessel wall requires a lower shear rate of only 200 s^{-1}.[5]

VWF fibers are anchored to the endothelium at a few distinct spots, allowing free waving of the fiber in the superfusing blood. P-selectin and αvβ3-integrins have been proposed as attachment points for

Submitted 7 November 2017; accepted 3 August 2018. DOI 10.1182/bloodadvances.2017013995.

*T.K. and T.M. contributed equally to this study.

The full-text version of this article contains a data supplement.

VWF fibers on the luminal surface of the endothelium.[7,8] However, the binding of VWF to P-selectin is negligible in the presence of physiological concentrations of calcium and magnesium.[7] Although the involvement of $\alpha\nu\beta3$-integrins has been clearly documented in vitro, additional binding partners have been proposed, given that surface-bound VWF fibers are still formed in β3-integrin knockout mice.[9]

Because VWF has a heparin binding site within the A1 domain, VWF fibers may be anchored to the endothelium through electrostatic interactions with negatively charged glycosaminoglycans (GAGs).[10] GAGs are part of the endothelial glycocalyx on the cellular surface. The composition of the endothelial glycocalyx is highly dynamic and strongly dependent on the vessel diameter, the vascular bed, and the surrounding microenvironment.[11] However, 50% to 90% of the endothelial glycocalyx may be composed of heparan sulfate (HS), whereas chondroitin sulfate and hyaluronan are less abundant.[11] The synthesis of HS involves a cascade of various enzymes, such as exostosin glycosyltransferases (Ext-1 and Ext-2). After its intracellular synthesis, HS is exposed by the membrane-bound HS proteoglycans of 2 protein families, the syndecans (SDCs) and the glypicans (GPs). GPs are attached to the plasma membrane through a glycosylphosphatidylinositol anchor and comprise 6 subtypes.[12] Endothelial cells express only GP-1.[12] The SDC family consists of 4 transmembrane proteins (SDC-1, -2, -3, and -4), all expressed by endothelial cells.[13] Aside from the expressional analysis of glycocalyx-related proteins, it is challenging to directly visualize the magnitude of the glycocalyx. In the present work, we applied label-free atomic force microscopy (AFM) to supplement lectin-based fluorescence staining. AFM enables the imaging of endothelial cells under physiological buffer conditions and provides morphological and physicochemical data with a nanometric resolution.[14]

Previously, it was reported that the expression of SDC-1 increases on endothelial cells during wound healing and in tumor blood vessels.[15] In the present study, we therefore applied an experimental melanoma model in mice to investigate whether SDC-1–exposed HS chains can anchor VWF fibers to the vessel wall. In microfluidic experiments mimicking physiological blood flow conditions, we analyzed the anchorage of VWF to the endothelial glycocalyx and to SDC-1 at the cellular level. Molecular binding kinetics were measured by flow cytometry and live-cell fluorescence microscopy.

Materials and methods

Additional information is available in the supplemental Data. All animal experiments were approved by the governmental animal care authorities.

In vivo experiments

Mouse *ret* transgenic melanoma cells, transfected with control short hairpin RNA (shRNA) or short hairpin heparanase (shHPSE) vectors (pRNAT-CMV3.1-Neo; GenScript USA Inc., Piscataway, NJ), were inoculated as a cell suspension (7.5 × 105 cells per 100 μL of phosphate-buffered saline [PBS]) intradermally to the dorsal skin of 10-week-old female C57BL/6 mice (n = 4 each group). After 2 weeks, the mice were euthanized, and the xenografts were resected, weighed, and fixed in Tissue-Tek (Sakura Finetek, Staufen, Germany) for cryosectioning.

Flow cytometry

HEK293 cells were detached from the culture flask using accutase (PAA, Pasching, Austria). The cell suspension was washed in PBS and incubated with enhanced green fluorescent protein–conjugated human recombinant VWF (rhVWF; kindly provided by R. Schneppenheim, Hamburg, Germany) for 20 min at 37°C in the dark. To remove nonbound VWF, HEK293 cells were washed with PBS twice and stored on ice in preparation for flow cytometry using a BD FACSCanto II.

Microfluidic experiments

An air pressure–based pump system (IBIDI GmbH, Munich, Germany) was used to induce laminar flow in microfluidic devices, as previously reported.[5] Briefly, human umbilical vein endothelial cells (HUVECs; 1×10^7 cells/cm^2) were grown on gelatin-coated μ-slides 0.2 Luer (IBIDI GmbH) for 48 hours under gentle flow (1 dyne/cm^2). Each slide was connected to the tubing of the pump system filled with *N*-2-hydroxyethylpiperazine-*N*′-2-ethanesulfonic acid (HEPES)–buffered Ringer's solution (140 mM of sodium chloride, 5 mM of potassium chloride, 1 mM of magnesium chloride, 1 mM of calcium chloride, 5 mM of glucose, and 10 mM of HEPES). The buffer contained 50 μM of histamine, 40% washed erythrocytes, and fluorescence-labeled platelets (4×10^6 cells per mL). Fluorescein isothiocyanate–conjugated VWF sheep anti-human antibody (Biozol, Eching, Germany) and Texas Red–conjugated wheat germ agglutinin (WGA) were used to stain VWF fibers and the endothelial glycocalyx in the course of the microfluidic experiment. Perfusion was performed with a shear stress of 6 dyne/cm^2 for 15 minutes. CellTrace calcein red-orange– or blue–labeled (Invitrogen, Darmstadt, Germany) platelets bound to VWF strings were detected in real time using a fluorescence microscope equipped with 20× and 40× oil objectives (Observer.Z1; Zeiss, Jena, Germany). Platelet-covered areas were quantified using imageJ v1.51.

AFM

HUVECs were imaged by AFM (The Nanowizard; JPK, Berlin, Germany) in contact mode, as previously described.[16] Briefly, HUVECs either remained untreated or were pretreated with 10 μg/mL of chitosan oligosaccharides (COSs) for 2 hours. Before imaging, HUVECs were fixed with 0.5% glutaraldehyde in HEPES-buffered Ringer's solution for 0.5 hours at room temperature. The applied cantilevers (CSC38; Micromash, Tallinn, Estonia) were characterized by a spring constant of 0.03 N/m. The acting loading force was <100 pN. Images were analyzed using Gwyddion software v2.47.

Statistical analysis

Results are expressed as means ± standard deviations of at least 3 independent experiments. Statistical significance was proven for multiple comparisons with 1-way analysis of variance followed by post hoc Bonferroni correction or for pairwise comparison with unpaired, 2-tailed Student *t* test. Spearman's rank correlation test was used to calculate the linear correlation coefficient. Calculations were conducted with SPSS software v24 and GraphPad Prism v7.03.

Results

Stabilization of the endothelial glycocalyx by COSs supports the formation of VWF fibers

To mimic pathophysiological conditions that facilitate VWF fiber formation on intact endothelial cells (Figure 1A), we stimulated HUVECs under laminar and continuous flow condition with 50 μM of histamine and in the absence of ADAMTS13 (a disintegrin and

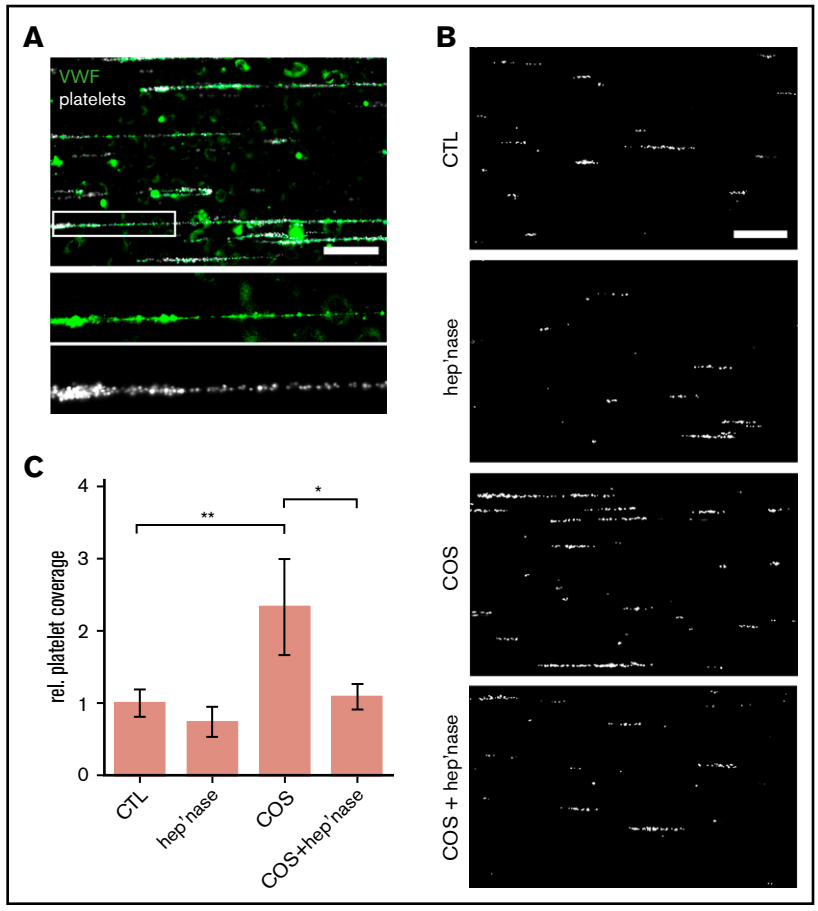

Figure 1. Binding of platelets to endothelial-released VWF. (A) Snapshot taken during a representative microfluidic experiment. HUVECs were perfused at a constant shear stress of 6 dyne/cm^2. VWF release was induced by 50 μM of histamine, and adhering fluorescent platelets (false color-coded in white) were tracked by fluorescence microscopy. VWF fibers (green) were stained with a FITC-conjugated antibody during the experiment. Scale bar, 100 μm. (B) VWF-mediated binding of platelets (white) to the endothelium. The endothelial gylcocalyx was manipulated through treatment with heparinase-I (hep'nase), COS, or both compounds (COS + hep'nase). Only histamine-treated HUVECs were used as control (CTL). Scale bar, 100 μm. (C) Quantitative evaluation of the VWF-dependent platelet coverage (n = 3-9). *$P \leq .05$, **$P \leq .01$ (1-way analysis of variance and Bonferroni post hoc test). rel., relative.

metalloproteinase with a thrombospondin type 1 motif member 13).[5] Under physiological conditions, ADAMTS13 inactivates VWF fibers rapidly through proteolysis. However, decreased plasma concentrations of ADAMTS13 in concert with increased amounts of VWF are found in infections and malignancy.[17-19] Lack of ADAMTS13 in the tumor microenvironment has been further attributed to the persistent development of intravascular VWF fibers in tumor blood vessels.[4]

In line with previous publications,[20,21] VWF fibers that were formed in our microfluidic channels firmly bound circulating platelets, producing a beads on a string–like configuration (Figure 1A). We were able to directly visualize the VWF fibers on top of the endothelial glycocalyx in real time during our microfluidic experiments through the addition of fluorescence-labeled anti-VWF antibodies and WGA lectins (supplemental Movies 1 and 2). Because this direct staining approach may prevent the proper formation of VWF strings and their hypothesized interaction with the glycocalyx, we perfused the endothelial cells in our quantitative experiments only with fluorescent platelets and no other labeling dye (Figure 1B). In those experiments, the platelet-covered area was a measure for the amount of VWF fibers formed on the surface of the endothelium.

To study the impact of the endothelial glycocalyx, we silenced Ext-1 expression, blocked HS by an antibody (supplemental Figure 1), removed cell surface–exposed HS chains with heparinase-I, or stabilized and protected the endothelial glycocalyx by pretreatment with COSs (Figure 1). Chitosan is a naturally occurring GAG, and we previously showed that chitosan binds heparin and interacts with the glycocalyx of epithelial cells.[22,23]

In comparison with control experiments (only histamine stimulation), the treatment of HUVECs with heparinase-I reduced the recruitment of platelets slightly, although the effect was not statistically significant (Figure 1B-C). A significant reduction of VWF-mediated platelet trapping was achieved through the knockdown of Ext-1 or the antibody blockage of HS (supplemental Figure 1A-B). In contrast, the pretreatment of HUVECs with COSs increased platelet string formation significantly (2.7- ± 0.34-fold; Figure 1 B-C). We performed VWF enzyme-linked immunosorbent assay to confirm that the increased VWF fiber formation on COS-treated HUVECs was not related to an increase in VWF secretion (supplemental Figure 2). Cotreatment of HUVECs with COSs and subsequently with heparinase prevented the COS-increased VWF-mediated platelet adhesion. Taken together, our findings indicate that HS is involved in the binding of VWF and that COSs are able to stabilize the HS-mediated anchorage of VWF fibers.

To further investigate the supposed modification of the endothelial cell surface by COSs, we applied AFM (Figure 2A). AFM provides nanometric-scale images and has been used to detect alterations of the glycocalyx.[24] In addition to the height information of the sample (height image), physicochemical changes on the surface (eg, changes in charge distribution) can be detected because they affect the contact time between the scanning tip and the surface (lateral deflection image).[25] In topographic overview images

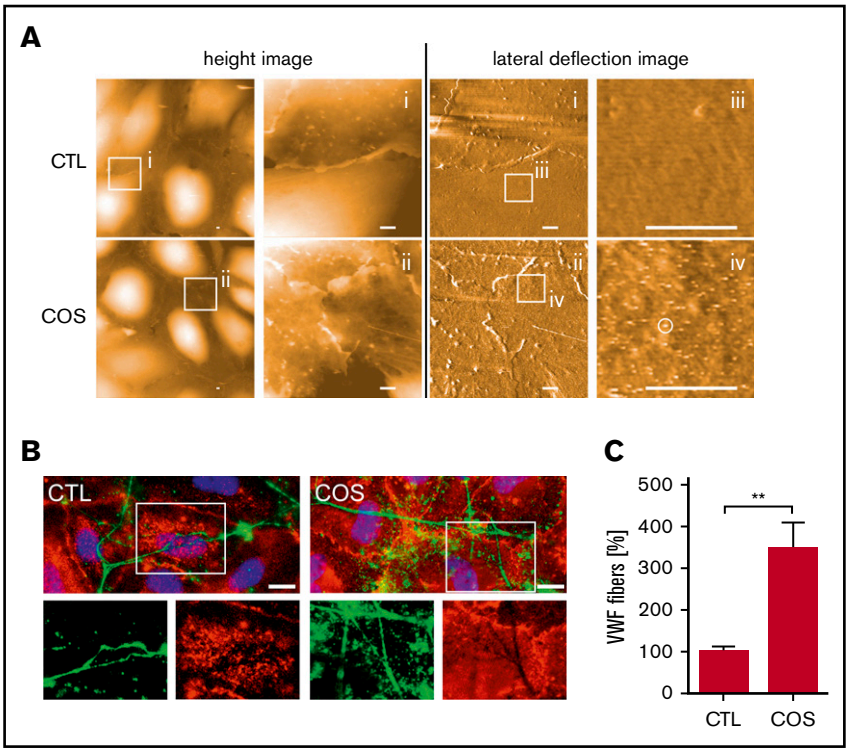

Figure 2. COS-induced modification of the endothelial glycocalyx promotes VWF binding. (A) Surfaces of HUVECs, treated with COSs (2μg/mL) or untreated (CTL), imaged by AFM. Height images provide 3-dimensional topography of the cellular surface. The height is false color coded. Black corresponds to a height of 0 μm and white to a height of 2 μm. Overview images are further magnified as indicated by square regions (i-ii). Corresponding lateral deflection images show the interaction between the scanning tip and the cellular surface in the depicted areas (i-ii). Further magnification of the lateral deflection images indicate an increased lateral deflection (white circle) on HUVECs treated with COSs in comparison with nontreated cells (CTL) (iii-iv). Scale bars, 1 μm. (B) Fluorescence microscopic analysis of the endothelial glycocalyx (red) and anchored VWF fibers (green). Cell nuclei are labeled in blue. The endothelial glycocalyx staining was more pronounced in COS-treated HUVECs. The lack of the endothelial glycocalyx staining beneath VWF fibers, which were in close proximity to the HUVEC surface, indicates an occupation of the HS chains by VWF. Scale bars, 10 μm. (C) Quantitative evaluations of VWF fluorescence staining of at least 10 fields of view of 3 independent experiments. $^{**}P \leq .01$ (Student *t* test).

(Figure 2A height image), we found that the treatment of HUVECs with COSs had no effect on general cell morphology. Furthermore, we also did not detect significant topographic alterations at the cellular surface at higher magnifications (Figure 2Ai-ii height image). However, at higher resolution using the lateral deflection mode (Figure 2Ai-iv lateral deflection image), we detected COS-induced alterations at the cellular surface, indicating a modification of the endothelial glycocalyx (Figure 2A white circle).

To further investigate the relevance of the endothelial glycocalyx in the anchorage of VWF fibers, we performed additional immunofluorescence-staining experiments on HUVECs (Figure 2B). The endothelial glycocalyx and VWF fibers were detected using Texas Red–conjugated WGA and a fluorescein isothiocyanate–labeled anti-VWF antibody, respectively. Figure 2B shows that VWF fibers were attached to endothelial cells. The endothelial glycocalyx was found to be nearly homogeneously distributed across the cellular surface, whereas pronounced levels were apparent at cellular junctions and at distinct spots on the cellular body (Figure 2B). Some distinct endothelial glycocalyx spots colocalized with VWF fibers (supplemental Figure 3), suggesting the glycocalyx-mediated anchorage of VWF.

However, more intriguing was the lack of WGA staining below VWF fibers that were in close proximity to the cellular surface (Figure 2B). The lack of staining might suggest that HS chains, in principle recognizable by WGA, are inaccessible because of their interaction with the VWF fibers. In line with our AFM data, HS staining was more pronounced on cells treated with COSs, confirming the stabilization of the endothelial glycocalyx. Quantitative evaluation of the VWF staining revealed 3.6 ± 0.61 times as many VWF fibers on COS-treated cells, indicating the better anchorage of VWF (Figure 2C). To further support our hypothesis of the endothelial glycocalyx–mediated tethering of VWF fibers, we performed additional in vivo experiments using an experimental melanoma model.

Colocalization of VWF and SDC-1 in vivo

Evidence of VWF fibers in vivo is rare.[26] One of the first experimental proofs of extended VWF fiber networks was described in inflamed liver vessels.[27] Recently, we reported the formation of VWF fiber networks in the lumen of blood vessels in malignant melanoma.[4]

Therefore, to obtain a quantifiable in vivo model, we generated primary tumors in mice by injecting *ret* transgenic melanoma cells intradermally into the dorsal skin. Substantial melanoma mass developed within 2 weeks, and tumors were dissected for ex vivo analysis. Our investigation focused on SDC-1, because previous reports suggested its upregulation in tumor blood vessels in connection to angiogenesis and vessel maturation.[15,28,29]

To further point out the potential contribution of SDC-1 in the anchorage of VWF, we investigated the coexpression of VWF and SDC-1 in tumoral and peritumoral tissues. Figure 3A shows a tissue cryosection stained for SDC-1 (red) and VWF (green). In peritumoral vessels, VWF is stored within the endothelial cells, indicating a nonactivated endothelium (Figure 3B). Moreover, there is a considerable amount of SDC-1 at the vessel wall, which colocalizes with VWF (Figure 3B). Quantitative analysis revealed a significant linear correlation between the expression of SDC-1 and VWF (Figure 3C). The coexistence of SDC-1 and VWF was further proven on the transcriptional level using public data representing 479 patients with melanoma provided by cBioPortal (Figure 3D).[30,31]

However, to prove that SDC-1–linked HS anchors VWF, we compared control melanoma cell (shCTL) tumors with shHPSE-deficient melanoma cell tumors (Figure 4A-B).[32] HPSE is capable

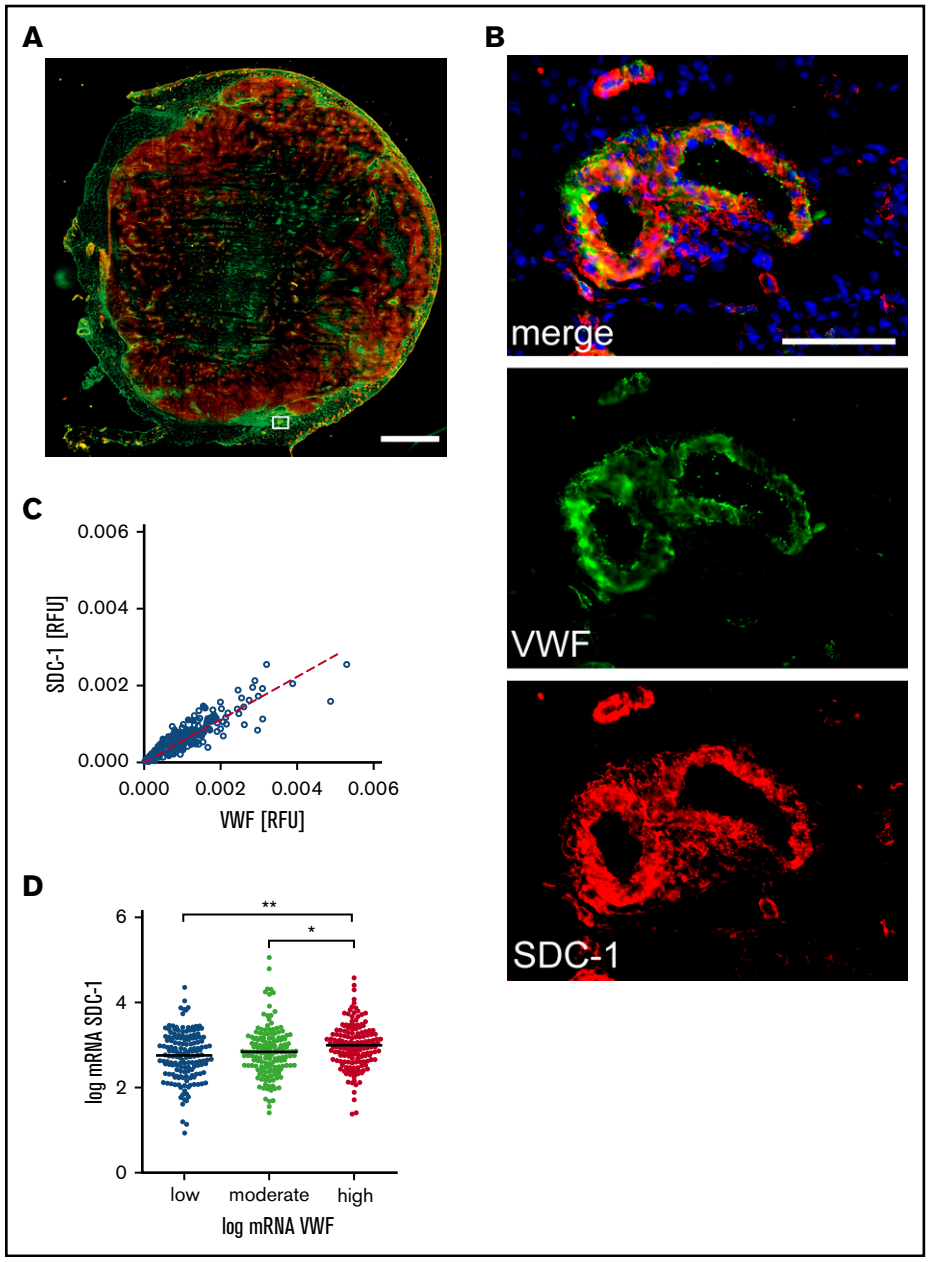

Figure 3. Coexpression of SDC-1 and VWF in melanoma tissue. (A) Representative overview image of a tumor tissue section comprising the primary melanoma and adjacent peritumoral skin. The image was assembled from 156 single immune fluorescence images. Scale bar, 2 mm. The white box marks a skin blood vessel adjacent to the melanoma tissue. The corresponding magnification is depicted in panel B. VWF is shown in green, SDC-1 in red, and cell nuclei in blue. Scale bar, 100 μm. (C) Colocalization of SDC-1 and VWF was quantified in 1649 blood vessels. The dashed line indicates the linear correlation between the expression of VWF and SDC-1. $R^2 = 0.87$; $P < .0001$ (Spearman's rank correlation). (D) Transcription analysis confirms correlation of SDC-1 and VWF expression in primary tumors of 479 patients with malignant melanoma. *$P \leq .05$, **$P \leq .01$ (1-way analysis of variance and Bonferroni post hoc test). mRNA, messenger RNA; RFU, relative fluorescence unit.

of trimming HS chains from proteoglycans such as SDC-1.[33] Furthermore, the removal of HS chains by HPSE strongly enhances proteolytic SDC-1 shedding caused, for example, by matrix metalloproteases (MMPs).[34,35] Accordingly, we suggest that silencing HPSE increases the ability of VWF to bind the endothelial glycocalyx and thus in turn increases the binding of VWF fibers. We found more SDC-1 in the blood vessels of shHPSE tumors compared with those of shCTL tumors, indicating that the HPSE-related shedding of SDC-1 is reduced when HPSE is silenced (Figure 4C left). In contrast, the average content of VWF per blood vessel was not significantly affected in either group (Figure 4C right).

To determine whether the presence of SDC-1 on the endothelium promotes the binding and accumulation of luminal VWF fiber networks, we compared tumor blood vessels in shCTL and shHPSE tumors (Figure 4A-B). The representative images indicate that the luminal distribution of VWF fiber networks was drastically affected when the shedding of SDC-1 was compromised (shHPSE). Quantitative analysis confirmed significantly more VWF networks bound to the vessel wall of shHPSE tumors compared with shCTL tumors (Figure 4D).

Although these findings already suggest the interaction between SDC-1 and VWF fiber networks, we aimed to translate the in vivo findings into our microfluidic setup. The transcriptional expression of SDC-1 in cultured HUVECs is low compared with the levels of SDC-2 to -4[13] (supplemental Figure 4). Therefore, to mimic pathophysiological conditions, we overexpressed SDC-1 in HUVECs by lentiviral transduction.

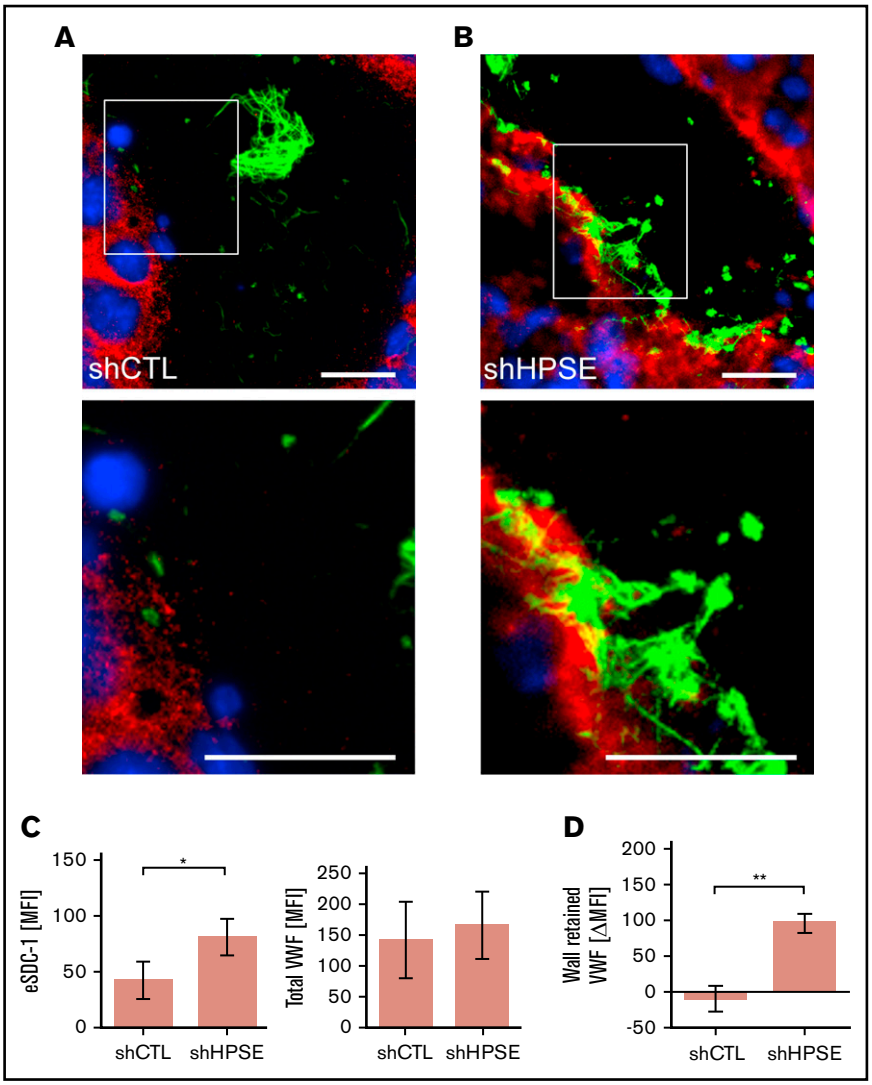

Figure 4. Interaction between endothelial SDC-1 and VWF fibers. Blood vessel of tumor tissue generated by control melanoma cells (shCTL) (A) or melanoma cells (B) with silenced HPSE (shHPSE). (A-B) White boxes mark the area of the depicted magnifications shown below. Scale bars, 20 μm. SDC-1 is shown in red, VWF in green, and nuclei in blue. (C) Quantifications of the endothelial SDC-1 (eSDC-1) and the total VWF content in shCTL and shHPSE tumors (n = 4). Signal levels were expressed as mean fluorescence intensity (MFI). (D) Change of VWF fiber amount retained at the blood vessel wall in shCTL and shHPSE tumors (n = 4). Differences in signal levels were expressed as change in MFI (ΔMFI). $^{*}P \leq .05$, $^{**}P \leq .01$ (Student *t* test).

SDC-1 promotes VWF fiber–mediated platelet binding in vitro

The expression and subcellular localization of SDC-1 after lentiviral transduction were confirmed by immunofluorescence staining (Figure 5A). In agreement with our quantitative reverse transcription polymerase chain reaction data, we detected only low levels of SDC-1 in HUVECs transfected with an EV. In contrast, there were substantially higher levels of SDC-1 on HUVECs transfected with the SDC-1 vector (SDC-1^{+}), and SDC-1 appeared in small clusters on the cellular surface (Figure 5A). We observed the increased clustering of SDC-1 at distinct points, frequently colocalizing with VWF fibers (Figure 5A magnified view). Analysis of the supernatants of HUVECs after stimulation with thrombin or histamine indicated that the overexpression of SDC-1 affected neither the reactivity of HUVECs nor the amount of VWF released (supplemental Figure 5).

Flow experiments were used to quantitatively confirm that the expression of SDC-1 promotes the binding of VWF fibers. Representative images acquired during live experiments show a pronounced formation of platelet strings on SDC-1^{+} HUVECs compared with the EV control (Figure 5B). On average, the area covered by platelets was 2.2 ± 0.27 times higher than in EV-transfected HUVECs. Treatment with heparinase-I reduced platelet binding to VWF fibers by 32.3% ± 6.94%, confirming that the binding induced by SDC-1 was dependent on HS (Figure 5C).

Colocalization of SDC-1 and VWF

In the next set of experiments, we aimed to visualize and quantify the interaction between SDC-1 and VWF. We therefore generated SDC-1^{+} HEK293 cells by expressing recombinant human SDC-1 fused to the red fluorescent protein DsRed. In comparison with EV-transfected cells, we measured a 26.4- ± 7.11-fold elevated SDC-1 expression. The expression of SDC-2, SDC-3, or SDC-4 was not affected by the genetic manipulation (supplemental Figure 6). The binding of exogenously added enhanced green fluorescent protein–tagged rhVWF to the surface of HEK293 cells was documented by fluorescence microscopy (Figure 6). We observed a clear colocalization of surface-bound VWF and the membranous SDC-1 (Figure 6A). For quantitative evaluation, we used flow cytometry. Here, the EV-transfected HEK293 cells showed only minor VWF-related fluorescence, whereas we detected a dose-dependent increase in VWF levels on the surface of SDC-1^{+}

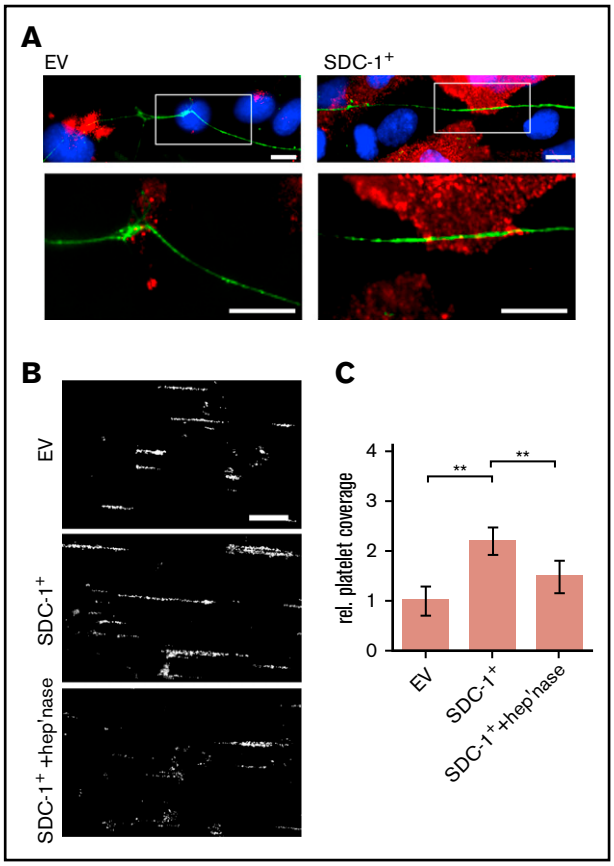

Figure 5. Interaction between endothelial SDC-1 and VWF fibers in vitro. (A) Representative images of empty vector (EV)–transfected HUVECs and cells that overexpress SDC-1 (SDC-1$^+$). Magnified regions (white boxes) are shown below. Scale bars, 10 μm. SDC-1 is shown in red, VWF in green, and nuclei in blue. (B) Endothelial SDC-1 promotes the VWF-mediated binding of platelets. HUVECs transfected with an EV control or with an SDC-1 vector (SDC-1$^+$) were perfused at a constant shear stress of 6 dyne/cm^2. VWF release was induced by 50 μM of histamine, and adhering fluorescent platelets were followed by fluorescence microscopy. Where indicated, the endothelial glycocalyx was trimmed by heparinase-I (hep'nase). Scale bar, 100 μm. (C) Quantitative evaluation of the VWF-dependent platelet coverage (n = 11). $^{**}P \leq .01$ (1-way analysis and Bonferroni post hoc test).

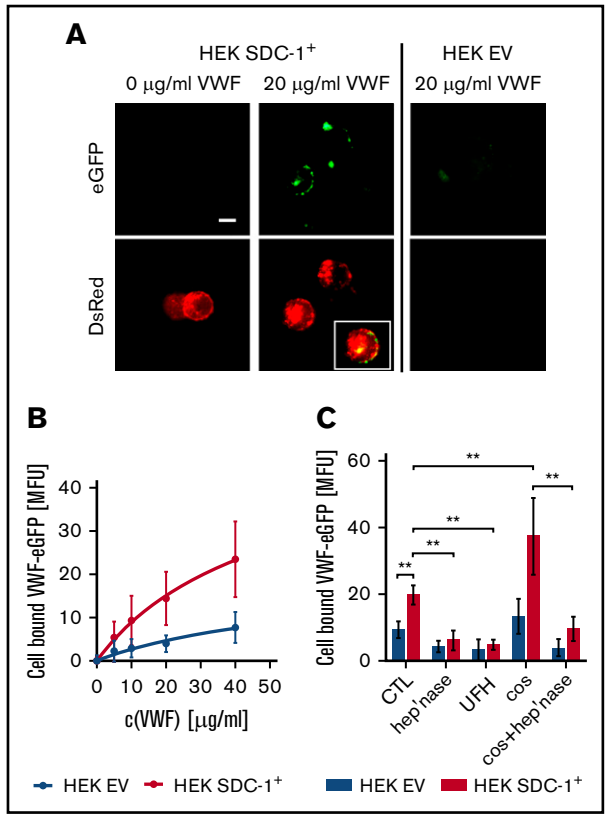

Figure 6. Interaction between recombinant VWF and recombinant SDC-1 exposed by HEK293 cells. (A) Fluorescence microscopic images of cells expressing human rhSDC-1 fused to the red fluorescent protein DsRed (SDC-1$^+$) were incubated with or without 20 μg/mL of enhanced green fluorescent protein (eGFP)–labeled human VWF. HEK293 cells that were transfected with an EV served as a control. Scale bar, 10 μm. Inset shows the colocalization between the VWF and membranous SDC-1. (B) Flow cytometric measurement of the dose-dependent binding of VWF to SDC-1$^+$ and EV cells (n = 3). (C) Binding of VWF to HEK cells in the presence of unfractionated heparin (UFH) or after manipulation of the glycocalyx with heparinase (hep'nase) and/or COS (n = 3-9). $^{**}P \leq .01$ (1-way analysis of variance and Bonferroni post hoc test).

HEK cells. Our measurements allowed us to estimate a dissociation constant (K_d) of ~180 nM (Figure 6B). The affinity of binding between GPIbα and the isolated A1 domain of VWF was comparable in magnitude (~30 nM),[36] suggesting a plausible interaction between SDC-1 and VWF. The impact of HS was proven through the action of heparinase-I and the addition of unfractionated heparin, both of which reduced the amount of bound VWF. In line with the data shown in Figures 1 and 2, treatment with COSs promoted VWF tethering, whereas cotreatment with heparinase abolished this effect (Figure 6C).

Discussion

In the present study, we identified the endothelial glycocalyx and more specifically HS chains exposed at the endothelial surface by proteoglycans such as SDC-1 as binding partners for VWF fibers. The endothelial glycocalyx has been proposed as a VWF anchorage point,[10] and binding of the chemically related heparin to the A1 domain of VWF has often been reported.[37-40]

Pathophysiological cooperation between SDC-1 and VWF has been documented in the liver of *Bacillus anthracis*–infected mice.[27] Vessel occlusions were related to the binding of platelets to VWF and endothelial-derived SDC-1 colocalized with thrombi in the central liver vein. However, these results prevent clear mechanistic conclusions, because the moribund animals experienced severe disseminated intravascular coagulation and extensive endothelial cell damage. We propose that the anchorage of VWF to endothelial SDC-1 is an early and temporary event, which occurs immediately after endothelial cell activation (Figure 7). Prolonged or excessive stimulation of the endothelium leading to endothelial cell damage also promotes the proteolytic removal of SDC-1 from the endothelial surface and may therefore counteract VWF anchorage.[41]

We generated primary melanomas characterized by well-defined disease progression and active luminal VWF secretion from the endothelium.[4,42] Our previous studies already suggested potential

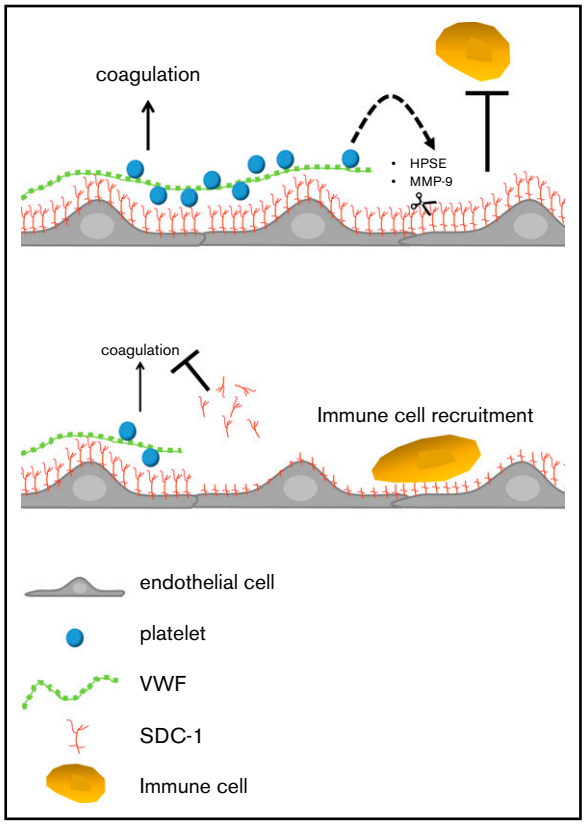

Figure 7. Proposed model aligning the obtained data to recent literature. VWF fibers are tethered to SDC-1 as part of the endothelial glycocalyx. Platelets are trapped by the VWF fibers and further activated in the course of coagulation (eg, through thrombin). Platelet-derived MMPs and HPSE are able to shed the endothelial glycocalyx. Soluble SDC-1 prevents further blood clotting, whereas the endothelial glycocalyx–free endothelial layer promotes the recruitment of immune cells.

cross talk between VWF and the endothelial glycocalyx because therapy with the low molecular–weight heparin tinzaparin blocked the formation of VWF fiber networks in tumor-bearing mice. Suppressed fiber formation was associated with a reduced tumor-cell progression, underlining the potential biological relevance of an endothelial glycocalyx–mediated anchorage of VWF. To further characterize the role of the endothelial glycocalyx and, more specifically, of HS on the binding of VWF fibers, we used melanoma-cell tumors deficient in HPSE. Lack of HPSE increased the levels of endothelial SDC-1 and concomitantly the number of vessel wall–attached VWF fibers (Figure 4).

Because our ex vivo analysis focused on SDC-1, we can only speculate about the effect of other proteoglycans. For instance, SDC-4 may additionally contribute to VWF anchorage. The lack of SDC-1 in SDC-1$^{-/-}$ mice is compensated by other proteoglycans such as SDC-4, indicating that the glycocalyx system is strongly redundant.[43] We also did not investigate the impact of other potential VWF binding partners, such as integrins. Interestingly, the treatment of SDC-1^{+} HUVECs with heparinase-I (Figure 5) significantly reduced the binding of platelets but did not reduce the formation of VWF-platelet strings down to control levels. These data suggest the existence of additional HS-independent binding mechanisms. Indeed, SDC-1 directly activates $\alpha\nu\beta3$-integrins via a defined peptide sequence within the SDC-1 protein, independently of HS.[44] Whether such activation could synergistically contribute to the direct anchorage of VWF fibers is still unclear but is a subject of our current research.

To provide further evidence for the direct interaction between SDC-1 and VWF, we overexpressed human recombinant SDC-1 in HEK293 cells and measured the binding of exogenously added VWF by flow cytometry and live-cell fluorescence microscopy (Figure 6). Similar to the experiments with HUVECs, COSs were able to support the anchorage of VWF. However, shedding of HS by heparinase was more efficient to attenuate VWF binding than in the experiments with HUVECs, suggesting a different cell type–dependent composition or stability of the glycocalyx.

Although the knowledge on the endothelial glycocalyx is steadily increasing, systematic research comparing different vascular beds, different physiological conditions, and temporal remodeling is to our knowledge still missing.[45] Because this lack of knowledge may impede clear mechanistic conclusions from in vivo experiments, we used in vitro microfluidic devices to analyze the molecular basis of the VWF fiber anchorage. However, the endothelial glycocalyx is supposed to be rapidly degraded in vitro.[46] It has been assumed that the glycocalyx of cultured endothelial cells measures only several nanometers, whereas in vivo, the thickness of the endothelial glycocalyx may range in the micrometer scale.[47] Accordingly, it is not surprising that the heparinase treatment of wild-type HUVECs showed only a small effect (Figure 1). To strengthen the conclusions of our in vitro experiments, we therefore increased the stability of the endothelial glycocalyx by COSs.

COSs are slightly positively charged at physiological pH and may bind to the negatively charged endothelial glycocalyx via electrostatic interactions.[22] To prove the presence of COSs at the endothelial layer and indicate a modification of the cellular surface, we used AFM. This imaging technique has been established by material scientists to detect, for example, charge distributions on nonbiological surfaces.[48] Although the physicochemical characterization of biological samples by AFM is less frequently reported,[49-51] we selected this method because the direct detection of cell-bound COSs by fluorescence microscopy failed (data not shown). AFM enabled us to measure an increased friction between the scanning probe and the endothelial cell surface after treatment with COSs (Figure 2A lateral deflection image). The applied loading force was minimal, suggesting that the increased friction was not related to a changed morphology but rather to locally restricted alterations of the charge distribution at the outer cellular surface. According to the counterion condensation theory, COS binding to the endothelial glycocalyx should not reduce the effective negative charge of the cellular surface.[52,53] However, it may protect the HS chains against degradation by mammalian HPSE during cell culture. Interestingly, the cotreatment of cells with COSs and the bacterial heparinase-I abrogated the protective effect of COSs (Figures 1C and 6C). Although this further indicates that the action of COSs is HS mediated, additional research on the glycocalyx-promoting mechanisms and the putative blockage of enzymatic degradation is required. Chitosan was also shown to directly inhibit the activity of proteoglycan-degrading MMPs,[54] which may also account for an improved stability of the glycocalyx.

Protection of the endothelial glycocalyx may offer a valuable therapeutic strategy to support vascular integrity during acute or

chronic vascular injuries.[55] Therefore, it might be of interest to show the potential of COSs as therapeutic agents to counteract vascular diseases such as reperfusion injury or bacteremia.

Figure 7 summarizes our findings and proposes a new molecular and mechanistic model in the light of recent literature. We showed that endothelial SDC-1 allows the local formation of platelet-decorated VWF fibers after acute stimulation (eg, by thrombin). Others have documented that thrombin can further activate VWF-bound platelets through PAR-1 or PAR-4 signaling.[56] Moreover, it is known that activated platelets release a plethora of effector molecules, including MMPs and HPSE.[57-60] These enzymes have been shown to orchestrate the shedding of endothelial SDC-1, leading to the release of soluble SDC-1 fragments.[35,61] These fragments can prevent extended blood clotting, which may help to maintain blood flow in the affected vasculature.[41] Blood flow is required to deliver immune cells to corresponding blood vessel sections, as a prerequisite for their site-specific recruitment. Additionally, because MMP- and HPSE-mediated shedding of the endothelial glycocalyx converts the endothelium into a proadhesive cell layer, immune cells can attach to and further infiltrate the tissue.[62]

In conclusion, we showed that endothelial SDC-1 facilitates the tethering of VWF fibers to the endothelium after acute stimulation in vitro or in the context of tumor-associated thrombosis. Surprisingly, little is known about the impact of surface-bound naturally occurring heparin/HS on blood clotting. Therefore, further research is required to better understand the cross talk between coagulation and bioactive carbohydrates. Detailed knowledge of the underlying molecular mechanisms will guide the tailor-made design of novel therapeutic heparins or heparin-like molecules with defined therapeutic actions, specifically blocking or promoting the anchorage of VWF fibers to blood vessel walls.

Acknowledgments

The authors thank Natalia Halter for excellent technical assistance.

This study was supported by the European Union's Seventh Framework Program for Research, Technological Development and Demonstration under grant agreement 613931 and the Deutsche Forschungsgemeinschaft within the RTG 2099, the IRTG 1549, SFB/Transregio 23, SHENC-Unit FOR 1543, and the knowledge-transfer project "Antibakterielle und abriebarme Beschichtung von Gleitflächen orthopädischer Implantate."

Authorship

Contribution: T.K., T.M., and C.G. performed experiments and analyzed and interpret data; Y.Y., K.I.P., A.F., L.C.-M., S.V.-y.-S., A.J., and A.T.B. performed experiments; and B.M.M., S.W.S., and C.G. designed the study and wrote the manuscript.

Conflict-of-interest disclosure: The authors declare no competing financial interests.

ORCID profile: T.M., 0000-0003-2736-7198.

Correspondence: Christian Gorzelanny, Medical Faculty Mannheim, Heidelberg University, Experimental Dermatology, Theodor-Kutzer-Ufer 1-3, 68167 Mannheim, Germany; e-mail: christian.gorzelanny@medma.uni-heidelberg.de or c.gorzelanny@uke.de.

REFERENCES

1. Huck V, Schneider MF, Gorzelanny C, Schneider SW. The various states of von Willebrand factor and their function in physiology and pathophysiology. *Thromb Haemost*. 2014;111(4):598-609.
2. Franco AT, Corken A, Ware J. Platelets at the interface of thrombosis, inflammation, and cancer. *Blood*. 2015;126(5):582-588.
3. Petri B, Broermann A, Li H, et al. von Willebrand factor promotes leukocyte extravasation. *Blood*. 2010;116(22):4712-4719.
4. Bauer AT, Suckau J, Frank K, et al. von Willebrand factor fibers promote cancer-associated platelet aggregation in malignant melanoma of mice and humans. *Blood*. 2015;125(20):3153-3163.
5. Pappelbaum KI, Gorzelanny C, Grässle S, et al. Ultralarge von Willebrand factor fibers mediate luminal Staphylococcus aureus adhesion to an intact endothelial cell layer under shear stress. *Circulation*. 2013;128(1):50-59.
6. Schneider SW, Nuschele S, Wixforth A, et al. Shear-induced unfolding triggers adhesion of von Willebrand factor fibers. *Proc Natl Acad Sci USA*. 2007;104(19):7899-7903.
7. Huang J, Roth R, Heuser JE, Sadler JE. Integrin alpha(v)beta(3) on human endothelial cells binds von Willebrand factor strings under fluid shear stress. *Blood*. 2009;113(7):1589-1597.
8. Padilla A, Moake JL, Bernardo A, et al. P-selectin anchors newly released ultralarge von Willebrand factor multimers to the endothelial cell surface. *Blood*. 2004;103(6):2150-2156.
9. Chauhan AK, Goerge T, Schneider SW, Wagner DD. Formation of platelet strings and microthrombi in the presence of ADAMTS-13 inhibitor does not require P-selectin or beta3 integrin. *J Thromb Haemost*. 2007;5(3):583-589.
10. De Ceunynck K, De Meyer SF, Vanhoorelbeke K. Unwinding the von Willebrand factor strings puzzle. *Blood*. 2013;121(2):270-277.
11. Reitsma S, Slaaf DW, Vink H, van Zandvoort MAMJ, oude Egbrink MG. The endothelial glycocalyx: composition, functions, and visualization. *Pflugers Arch*. 2007;454(3):345-359.
12. Weinbaum S, Tarbell JM, Damiano ER. The structure and function of the endothelial glycocalyx layer. *Annu Rev Biomed Eng*. 2007;9:121-167.
13. Vuong TT, Reine TM, Sudworth A, Jenssen TG, Kolset SO. Syndecan-4 is a major syndecan in primary human endothelial cells in vitro, modulated by inflammatory stimuli and involved in wound healing. *J Histochem Cytochem*. 2015;63(4):280-292.
14. Schneider SW, Yano Y, Sumpio BE, et al. Rapid aldosterone-induced cell volume increase of endothelial cells measured by the atomic force microscope. *Cell Biol Int*. 1997;21(11):759-768.
15. Götte M. Syndecans in inflammation. *FASEB J*. 2003;17(6):575-591.

16. Bauer AT, Strozyk EA, Gorzelanny C, et al. Cytotoxicity of silica nanoparticles through exocytosis of von Willebrand factor and necrotic cell death in primary human endothelial cells. *Biomaterials*. 2011;32(33):8385-8393.

17. O'Sullivan JM, Preston RJ, O'Regan N, O'Donnell JS. Emerging roles for hemostatic dysfunction in malaria pathogenesis. *Blood*. 2016;127(19): 2281-2288.

18. Ono T, Mimuro J, Madoiwa S, et al. Severe secondary deficiency of von Willebrand factor-cleaving protease (ADAMTS13) in patients with sepsis-induced disseminated intravascular coagulation: its correlation with development of renal failure. *Blood*. 2006;107(2):528-534.

19. Franchini M, Frattini F, Crestani S, Bonfanti C, Lippi G. von Willebrand factor and cancer: a renewed interest. *Thromb Res*. 2013;131(4):290-292.

20. Dong JF, Moake JL, Nolasco L, et al. ADAMTS-13 rapidly cleaves newly secreted ultralarge von Willebrand factor multimers on the endothelial surface under flowing conditions. *Blood*. 2002;100(12):4033-4039.

21. De Ceunynck K, Rocha S, Feys HB, et al. Local elongation of endothelial cell-anchored von Willebrand factor strings precedes ADAMTS13 protein-mediated proteolysis. *J Biol Chem*. 2011;286(42):36361-36367.

22. Kaiser M, Pereira S, Pohl L, et al. Chitosan encapsulation modulates the effect of capsaicin on the tight junctions of MDCK cells. *Sci Rep*. 2015;5:10048.

23. Grässle S, Huck V, Pappelbaum KI, et al. von Willebrand factor directly interacts with DNA from neutrophil extracellular traps. *Arterioscler Thromb Vasc Biol*. 2014;34(7):1382-1389.

24. Lydataki S, Lesniewska E, Tsilimbaris MK, et al. Observation of the posterior endothelial surface of the rabbit cornea using atomic force microscopy. *Cornea*. 2003;22(7):651-664.

25. Schneider SW, Egan ME, Jena BP, Guggino WB, Oberleithner H, Geibel JP. Continuous detection of extracellular ATP on living cells by using atomic force microscopy. *Proc Natl Acad Sci USA*. 1999;96(21):12180-12185.

26. André P, Denis CV, Ware J, et al. Platelets adhere to and translocate on von Willebrand factor presented by endothelium in stimulated veins. *Blood*. 2000;96(10):3322-3328.

27. Popova TG, Millis B, Bailey C, Popov SG. Platelets, inflammatory cells, von Willebrand factor, syndecan-1, fibrin, fibronectin, and bacteria co-localize in the liver thrombi of Bacillus anthracis-infected mice. *Microb Pathog*. 2012;52(1):1-9.

28. Beauvais DM, Ell BJ, McWhorter AR, Rapraeger AC. Syndecan-1 regulates alphavbeta3 and alphavbeta5 integrin activation during angiogenesis and is blocked by synstatin, a novel peptide inhibitor. *J Exp Med*. 2009;206(3):691-705.

29. Orecchia P, Conte R, Balza E, et al. A novel human anti-syndecan-1 antibody inhibits vascular maturation and tumour growth in melanoma. *Eur J Cancer*. 2013;49(8):2022-2033.

30. Gao J, Aksoy BA, Dogrusoz U, et al. Integrative analysis of complex cancer genomics and clinical profiles using the cBioPortal. *Sci Signal*. 2013;6(269):pl1.

31. Cerami E, Gao J, Dogrusoz U, et al. The cBio cancer genomics portal: an open platform for exploring multidimensional cancer genomics data. *Cancer Discov*. 2012;2(5):401-404.

32. Yang Y, Gorzelanny C, Bauer AT, et al. Nuclear heparanase-1 activity suppresses melanoma progression via its DNA-binding affinity. *Oncogene*. 2015; 34(47):5832-5842.

33. Purushothaman A, Uyama T, Kobayashi F, et al. Heparanase-enhanced shedding of syndecan-1 by myeloma cells promotes endothelial invasion and angiogenesis. *Blood*. 2010;115(12):2449-2457.

34. Yang Y, Macleod V, Miao HQ, et al. Heparanase enhances syndecan-1 shedding: a novel mechanism for stimulation of tumor growth and metastasis. *J Biol Chem*. 2007;282(18):13326-13333.

35. Jung O, Trapp-Stamborski V, Purushothaman A, et al. Heparanase-induced shedding of syndecan-1/CD138 in myeloma and endothelial cells activates VEGFR2 and an invasive phenotype: prevention by novel synstatins. *Oncogenesis*. 2016;5:e202.

36. Huizinga EG, Tsuji S, Romijn RA, et al. Structures of glycoprotein Ibalpha and its complex with von Willebrand factor A1 domain. *Science*. 2002; 297(5584):1176-1179.

37. Sobel M, Soler DF, Kermode JC, Harris RB. Localization and characterization of a heparin binding domain peptide of human von Willebrand factor. *J Biol Chem*. 1992;267(13):8857-8862.

38. Sobel M, McNeill PM, Carlson PL, et al. Heparin inhibition of von Willebrand factor-dependent platelet function in vitro and in vivo. *J Clin Invest*. 1991; 87(5):1787-1793.

39. Sixma JJ, Schiphorst ME, Verweij CL, Pannekoek H. Effect of deletion of the A1 domain of von Willebrand factor on its binding to heparin, collagen and platelets in the presence of ristocetin. *Eur J Biochem*. 1991;196(2):369-375.

40. Fujimura Y, Titani K, Holland LZ, et al. A heparin-binding domain of human von Willebrand factor. Characterization and localization to a tryptic fragment extending from amino acid residue Val-449 to Lys-728. *J Biol Chem*. 1987;262(4):1734-1739.

41. Larsen AM, Leinøe EB, Johansson PI, Birgens H, Ostrowski SR. High syndecan-1 levels in acute myeloid leukemia are associated with bleeding, thrombocytopathy, endothelial cell damage, and leukocytosis. *Leuk Res*. 2013;37(7):777-783.

42. Goertz L, Schneider SW, Desch A, et al. Heparins that block VEGF-A-mediated von Willebrand factor fiber generation are potent inhibitors of hematogenous but not lymphatic metastasis. *Oncotarget*. 2016;7(42):68527-68545.

43. McDermott SP, Ranheim EA, Leatherberry VS, Khwaja SS, Klos KS, Alexander CM. Juvenile syndecan-1 null mice are protected from carcinogen-induced tumor development. *Oncogene*. 2007;26(10):1407-1416.

44. Beauvais DM, Burbach BJ, Rapraeger AC. The syndecan-1 ectodomain regulates alphavbeta3 integrin activity in human mammary carcinoma cells. *J Cell Biol*. 2004;167(1):171-181.

45. Dane MJ, van den Berg BM, Lee DH, et al. A microscopic view on the renal endothelial glycocalyx. *Am J Physiol Renal Physiol*. 2015;308(9):F956-F966.

46. Chappell D, Jacob M, Paul O, et al. The glycocalyx of the human umbilical vein endothelial cell: an impressive structure ex vivo but not in culture. *Circ Res*. 2009;104(11):1313-1317.

47. Ebong EE, Macaluso FP, Spray DC, Tarbell JM. Imaging the endothelial glycocalyx in vitro by rapid freezing/freeze substitution transmission electron microscopy. *Arterioscler Thromb Vasc Biol*. 2011;31(8):1908-1915.

48. Bampoulis P, Sotthewes K, Siekman MH, Zandvliet HJ, Poelsema B. Graphene visualizes the ion distribution on air-cleaved mica. *Sci Rep*. 2017;7:43451.

49. Girasole M, Cricenti A, Generosi R, et al. Different membrane modifications revealed by atomic force/lateral force microscopy after doping of human pancreatic cells with Cd, Zn, or Pb. *Microsc Res Tech*. 2007;70(10):912-917.

50. Melling M, Karimian-Teherani D, Behnam M, Mostler S. Morphological study of the healthy human oculomotor nerve by atomic force microscopy. *Neuroimage*. 2003;20(2):795-801.

51. Dean D, Hemmer J, Vertegel A, Laberge M. Frictional behavior of individual vascular smooth muscle cells assessed by lateral force microscopy. *Materials (Basel)*. 2010;3(9):4668-4680.

52. Manning GS. Limiting laws and counterion condensation in polyelectrolyte solutions. I. Colligative properties. *J Chem Phys*. 1969;51(3):924-933.

53. Wedlock DJ, Diakun GP, Edwards HE, Phillips GO, Allen JC. An investigation of calcium ion binding to heparins. *Biochim Biophys Acta*. 1980;629(3):530-538.

54. Gorzelanny C, Pöppelmann B, Strozyk E, Moerschbacher BM, Schneider SW. Specific interaction between chitosan and matrix metalloprotease 2 decreases the invasive activity of human melanoma cells. *Biomacromolecules*. 2007;8(10):3035-3040.

55. Becker BF, Chappell D, Bruegger D, Annecke T, Jacob M. Therapeutic strategies targeting the endothelial glycocalyx: acute deficits, but great potential. *Cardiovasc Res*. 2010;87(2):300-310.

56. Etulain J, Mena HA, Negrotto S, Schattner M. Stimulation of PAR-1 or PAR-4 promotes similar pattern of VEGF and endostatin release and pro-angiogenic responses mediated by human platelets. *Platelets*. 2015;26(8):799-804.

57. Freeman C, Parish CR. Human platelet heparanase: purification, characterization and catalytic activity. *Biochem J*. 1998;330(Pt 3):1341-1350.

58. Cecchetti L, Tolley ND, Michetti N, Bury L, Weyrich AS, Gresele P. Megakaryocytes differentially sort mRNAs for matrix metalloproteinases and their inhibitors into platelets: a mechanism for regulating synthetic events. *Blood*. 2011;118(7):1903-1911.

59. Mannello F, Medda V. Differential expression of MMP-2 and MMP-9 activity in megakaryocytes and platelets. *Blood*. 2011;118(24):6470-6471, author reply 6471-6473.

60. Sawicki G, Sanders EJ, Salas E, Wozniak M, Rodrigo J, Radomski MW. Localization and translocation of MMP-2 during aggregation of human platelets. *Thromb Haemost*. 1998;80(5):836-839.

61. Manon-Jensen T, Multhaupt HAB, Couchman JR. Mapping of matrix metalloproteinase cleavage sites on syndecan-1 and syndecan-4 ectodomains. *FEBS J*. 2013;280(10):2320-2331.

62. Kharabi Masouleh B, Ten Dam GB, Wild MK, et al. Role of the heparan sulfate proteoglycan syndecan-1 (CD138) in delayed-type hypersensitivity. *J Immunol*. 2009;182(8):4985-4993.